Journal of MATERIALS RESEARCH

Invited Feature Paper - Review
DOI: 10.1557/jmr.2019.167

Double resonance Raman scattering process in 2D materials

Rafael N. Gontijo[1], Geovani C. Resende[1], Cristiano Fantini[1], Bruno R. Carvalho[2,a)]

[1]Departamento de Física, Universidade Federal de Minas Gerais, Belo Horizonte, Minas Gerais 30123-970, Brazil
[2]Departamento de Física, Universidade Federal do Rio Grande do Norte, Natal, Rio Grande do Norte 59078-970, Brazil
[a)]Address all correspondence to this author. e-mail: brunorc@fisica.ufrn.br
This paper has been selected as an Invited Feature Paper.

Received: 9 January 2019; accepted: 22 April 2019

Raman spectroscopy is a fundamental tool for the characterization of two-dimensional materials. It provides insights into the electronic and vibrational properties of these materials and is particularly rich in features when the incident laser energy approaches the electronic energy transition of the material. Among these features, the double resonance Raman process provides important information on the electron, phonon, and electron–phonon properties. It was on the study of carbon-related materials that the double resonance bands sparkled showing their potential and, since then, have been deeply searched in the study of novel 2D materials. Here, the authors review the double resonance Raman process in 2D materials focusing on graphene and semiconducting MoS_2 highlighting the origin of the bands mediated by the two-phonon and phonon–defect processes. The authors discuss the observed properties of the double resonance bands and compare the processes for graphene and MoS_2 to find guiding principles for the appearance of double resonance bands. The authors also discuss the new findings of the intervalley scattering process in transition metal dichalcogenides. A brief discussion of the defect-induced bands in both materials is also presented.

Introduction

In the past years, Raman spectroscopy has presented itself as a key tool to obtain information about structure and physical properties of 2D materials. It can provide better understanding of the electronic and vibrational properties in several types of 2D systems such as graphene [1, 2, 3], black phosphorus [4], hexagonal boron nitride [5, 6, 7], and transition metal dichalcogenides (TMDs) [8, 9]. The analysis of the Raman spectrum of TMDs, for instance, allows us to gather information about the interlayer interactions [10], spin–orbit splitting [11], exciton–phonon interactions [12, 13, 14], as well as dependence of the phonon frequencies with the number of layers [15, 16, 17, 18, 19, 20, 21, 22], among many other relevant characteristics that are fundamental to unveil the underlying physics in these systems [10, 23, 24, 25, 26]. In addition, Raman spectroscopy can probe the intravalley and interlayer phonon interactions in twisted bilayer heterostructures, where new Raman bands arise due to periodic potentials of Moiré patterns that create allowed states in inner points of the Brillouin zone [27, 28].

Of special interest is the observation of second-order double resonance Raman bands in 2D materials. Double resonance bands have been used in the literature to obtain important information from III–V group semiconductors [29, 30, 31], cadmium telluride alloy [32], graphite and graphene [2, 3, 33, 34, 35, 36, 37, 38, 39, 40, 41, 42, 43], and extensive studies from bulk to monolayer regimes of TMDs as well [11, 14, 21, 22, 44, 45, 46, 47, 48, 49, 50, 51, 52, 53, 54, 55, 56, 57, 58]. The double resonance process arises from the intervalley or intravalley scattering where two phonons or one phonon and one defect participate in the scattering of the excited electron. The double resonance bands can help us characterize both electronic and vibrational properties of these materials. These contributions can aid in the understanding of changes in basic properties brought by defects, which could in turn allow the application of 2D materials to new relevant technologies [59, 60].

The first-order Raman scattering only allows the observation of phonons at the Brillouin zone center (the Γ point). This is justified by the fact that the momentum carried by light is

https://doi.org/10.1557/jmr.2019.167 Published online by Cambridge University Press

© Materials Research Society 2019

much smaller than the size of the Brillouin zone and, consequently, much smaller than the momentum required to reach phonons away from the **Γ** point. Therefore, the optical transitions can be regarded as strictly vertical [61]. The second requirement is that the irreducible representations must transform as quadratic base functions [2, 8, 9]. Semiconducting monolayer TMDs such as MoS_2, with trigonal prismatic symmetry, belong to the D_{3h} point group, which predicts two Raman active modes, A_1' and E', in the backscattering configuration [9]. Thus, only two peaks can be seen in their first-order Raman spectrum.

Figure 1(a) represents the Raman process (Stokes) when one phonon is participating in the inelastic scattering process of a photon in a parabolic band semiconductor (first-order process). Here, a photon with energy $\hbar\omega$ impinging on the hypothetical material creates an electron–hole pair, promoting the electron from the initial state $|i\rangle$ to an excited state $|a\rangle$ through an electron–radiation interaction (H_{e-R}). This is a similar process to light absorption. Then, the excited electron interacts with the crystal lattice (electron–phonon interaction, H_{e-Ph}) and goes to the state $|b\rangle$ by emitting a phonon of energy $\hbar\omega_{Ph}$. Finally, the electron–hole pair recombines by emitting a photon with energy equal to $\hbar\omega - \hbar\omega_{Ph}$, going to the final state $|f\rangle$ through another electron–radiation interaction. The equation of the Raman process that describes the relation between incoming and outgoing photon energies and its intensity is given by [12]

$$I(\hbar\omega) = \sum_{a,b} \left| \frac{\langle f|H_{e-R}|b\rangle\langle b|H_{e-Ph}|a\rangle\langle a|H_{e-R}|i\rangle}{(\hbar\omega - E_X + i\gamma)(\hbar\omega - \hbar\omega_{Ph} - E_X + i\gamma)} \right|^2 , \quad (1)$$

where E_X is the optical transition energy of the material and γ is inversely proportional to the lifetime of the Raman process. If the incoming photon energy is equal to either E_X or $E_X + \hbar\omega_{Ph}$, the process is resonant and the intensities of the Raman modes are strongly enhanced. Therefore, Eq. (1) is essential to the study of all 2D materials, because it provides information on the electron–phonon interactions.

Meanwhile, two-phonon Raman bands obey different selection rules, which do not only consider vertical transitions but also the scattering of the excited electron throughout the entire reciprocal lattice as long as momentum conservation is achieved [1, 36, 50]. The intensity of the two-phonon bands can be described by the following equation:

$$I(\hbar\omega) = \sum_{a,b,c} \left| \frac{\langle f|H_{e-R}|c\rangle\langle c|H_{e-Ph'}|b\rangle\langle b|H_{e-Ph}|a\rangle\langle a|H_{e-R}|i\rangle}{(\hbar\omega - E_X + i\gamma)(\hbar\omega - \hbar\omega_{Ph} - E_X + i\gamma)(\hbar\omega - \hbar\omega_{Ph'} - \hbar\omega_{Ph} - E_X + i\gamma)} \right|^2 . \quad (2)$$

Notice the presence of a second electron–phonon interaction and a third intermediate state, $|c\rangle$, due to the creation of a second phonon with energy $\hbar\omega_{Ph'}$, in contrast with Eq. (1). Figure 1(b) illustrates a two-phonon process. First, similar to the first-order process, the electron is promoted from the

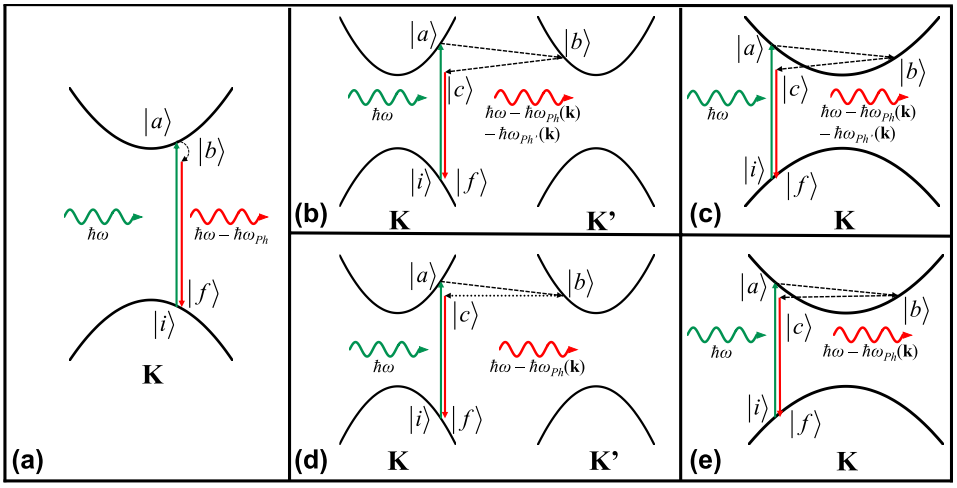


Figure 1: First-order and double resonance Raman scattering. (a) Schematic of the first-order resonant Raman scattering process in a parabolic band semiconductor. First, an electron is excited from the valence band ($|i\rangle$) to the conduction band ($|a\rangle$) by a photon with energy $\hbar\omega$. The interaction between electron and lattice emits a phonon close to the **Γ** point with energy $\hbar\omega_{Ph}$ ($|b\rangle$). When the excited electron recombines with the hole in the valence band, a photon is emitted with energy $\hbar\omega - \hbar\omega_{Ph}$ ($|f\rangle$). (b) Schematic of a two-phonon intervalley scattering. After the electron is excited to the conduction band ($|a\rangle$), a phonon with momentum **k**, represented by the dashed line, scatters the excited electron to the **K**′ valley band ($|b\rangle$). To conserve momentum, the electron is scattered back to **K** valley by another phonon with wavevector $-\mathbf{k}$ ($|c\rangle$). After the recombination of electron–hole pair, a photon is emitted with energy $\hbar\omega - \hbar\omega_{Ph}(\mathbf{k}) - \hbar\omega_{Ph'}(\mathbf{k})$. (c) Schematic of a two-phonon intravalley scattering. The same states from the intervalley scattering are observed, only now the scattering happens along the same valley. (d) Schematic of a phonon–defect intervalley scattering process, where a defect, represented by the dotted line, scatters the electron back to the **K** valley. (e) Schematic of a phonon–defect intravalley scattering. This is the representation of a hypothetical material intended for illustration purposes only. All scales have been exaggerated for clarity.

https://doi.org/10.1557/jmr.2019.167 Published online by Cambridge University Press

© Materials Research Society 2019

valence band (state $|i\rangle$) to the conduction band (state $|a\rangle$) and it interacts with the lattice to emit a phonon with energy $\hbar\omega_{Ph}$ (state $|b\rangle$). However now, instead of a zone center phonon, the emitted phonon has enough momentum to scatter the electron from one point in the Brillouin zone to another (**K** to **K′** in our example). To guarantee momentum conservation, the electron at **K′** must emit another phonon with the same amount of momentum that the first phonon had and energy $\hbar\omega_{Ph'}$ (state $|c\rangle$). Finally, the excited electron–hole pair recombines and a photon with energy equal to $\hbar\omega - \hbar\omega_{Ph} - \hbar\omega_{Ph'}$ is emitted. Due to the scattering of the electron from one valley to the other, this process is frequently called intervalley scattering [50]. Another example of two-phonon process could be the intravalley scattering, where instead of the electron being scattered from the **K** valley to the **K′** valley, the electron is scattered in the same valley, following the same trajectory as Fig. 1(c). The same procedures from intervalley process can be applied, just the length of the wavevector changes.

One could ask the question of how would defects change the Raman process. Figures 1(d) and 1(e) present the defect-induced Raman process expected for a low-defective material (a material with a defect density low enough that its basic properties are not very affected by defects). In this case, the same process for intervalley and intravalley scatterings occur, but the transition from state $|b\rangle$ to state $|c\rangle$ is carried by a defect instead of a phonon. Then, the energy of the scattered photon will be $\hbar\omega - \hbar\omega_{Ph}$, like in the case of the first-order bands, but the phonon participating in the Raman process is not a zone-center phonon. The intensity of this process can be explained by means of Eq. (2) as well [35], after some minor changes to include the electron–defect interaction.

The processes illustrated in Figs. 1(b)–1(e) have only shown the scattering of the electron from one point to the other in the electronic structure. As a matter of fact, the electron is not the only entity that can be scattered, but the hole in the valence band can be scattered as well [11, 42]. For the case where the electron is the only entity scattered in an intervalley or intravalley process, we call it electron–electron scattering. If both electron and hole are scattered, we call it electron–hole scattering and the case where just the hole is scattered can be called hole–hole scattering.

Unfortunately, the two-phonon bands have very low probability of happening, such that their intensity is much smaller than that of first-order modes. Nevertheless, when the incoming laser energy reaches resonance with the electronic transition of the material, or when the defect density is high enough, the intensity becomes comparable or even higher than that of the first-order modes [43, 50, 62, 63]. When it happens, the bands approach a resonant behavior like that of the first-order modes. But, since the choices are not limited to the zone-center phonons, other terms in the denominator of Eq. (2) can be null at the same time. That is why these bands are called double resonance bands or even triple resonance bands in some cases [50, 64].

In this review, we present some of the recent advances on the double resonance Raman process in two dimensional materials. We also discuss some information that can be obtained from the analysis of the double resonance Raman bands and its applications, e.g., investigation of defects in 2D materials. We start by revising the double resonance process in graphene and follow up with the recent findings in TMDs, in particular for MoS_2. Further, a perspective of possible future studies for other classes of 2D materials is presented.

Double resonance Raman process

The appearance of double resonance Raman bands can be originated by an intervalley scattering of the excited electron by a combination of two phonons of same wavevectors but with opposite signs. The process is resonant if at least one of the states accessed by the electron is a real electronic state. However, the double resonance process is characterized by two real states connecting each other [2, 38]. It can be either a band state in the conduction band, such as in the case of graphene, or it can be an excitonic state, such as in the case of TMDs. The phonons that participate in the process will be limited to those with wavevectors that can connect states with similar energy of the excited electron [2, 38]. Such is the case for the D and 2D bands in the Raman spectrum of graphene. These bands arise from the contributions of the TO branch around the **K** point [see Fig. 2(a)] [1]. In the case of the MoS_2, a semiconducting TMD, it has been recently demonstrated that the double resonance band in the material has contributions from the longitudinal acoustic (LA) and transversal acoustic (TA) phonon branches in the vicinities of the **K** and **M** points [see Fig. 2(b)] [8, 49]. The aforementioned considerations help us to understand some rules regarding the double resonance process and, the information that it can provide, such as the electron or phonon velocity along a certain region in the electron or phonon dispersion [3]. In the next sections, we address some physical properties of graphene and TMDs focusing mainly on their electronic and vibrational properties, which are essential for understanding the observed double resonance bands in these materials [8, 50].

Graphene

Graphene was the first isolated 2D material, and it is regarded as the strongest material due to its in-plane double sp^2 bonding [65]. At the same time, it was one of the first 2D materials to have its Raman spectra measured [1].

The electronic properties of graphene can be well described by the tight binding approach considering two p_z orbitals [66].

https://doi.org/10.1557/jmr.2019.167 Published online by Cambridge University Press

© Materials Research Society 2019

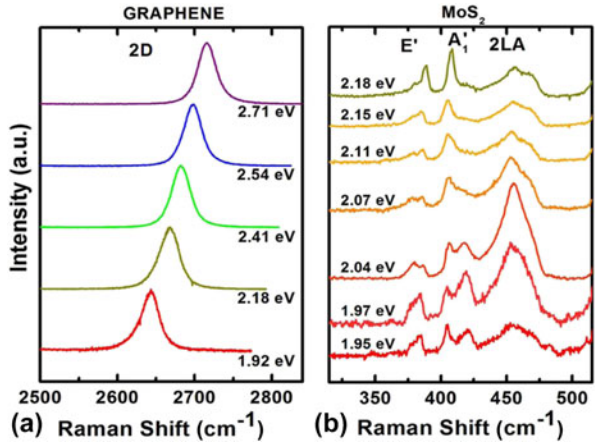


Figure 2: The two-phonon Raman bands. Comparison between the double resonance intervalley scattering in (a) graphene and (b) monolayer MoS_2. Reprinted with permission from Ref. 8.

Thus, the one electron dispersion of graphene is characterized by the presence of Dirac cones near the **K** point in the Brillouin zone, where the valence and conduction bands touch each other, making graphene be considered a zero band gap semiconductor [67]. In a first approximation, the electronic band structure around the **K** point can be regarded as linear and, consequently, the dependence of the electronic density of states presents a linear behavior near the Fermi level [68]. The optical transitions in graphene are characterized by vertical transitions from valence band to the conduction band close to the **K** point, with constant light absorption in the near infrared (NIR) and visible spectral regions [69]. As for the vibrational properties of graphene, there are six phonon branches at the **Γ** point, three acoustic and three optical phonon branches, named longitudinal acoustic (LA), transversal acoustic (TA), and out of plane transversal acoustic (ZA); out of plane transversal optic (ZO), longitudinal optic (LO), and transversal optic (TO). Among these phonon branches, only the LO and TO modes at the **Γ** point are Raman active and correspond to a degenerate E_{2g} representation (the G band). Thus, the expected Raman spectrum should consist of a single first-order band.

Nevertheless, the Raman spectrum of pristine graphene is characterized by the presence of mostly four bands, named as G, D + D″, 2D, and 2D′ in frequency order [Fig. 3(a)] [3]. In the presence of defects, new features arise in the Raman spectrum of graphene; thus, besides the four Raman bands observed in a pristine graphene, three other bands are also observed, named as D, D′, and D + D′ [see Fig. 3(a)].

The G band (the E_{2g} mode) originates from a first-order Raman process, as shown in Fig. 1(a). As a first-order process, it will be present in the Raman spectrum of pristine and defective samples regardless of the excitation laser energy and number of layers [1, 2, 43, 70, 71, 72]. An interesting aspect of the G band is its classical behavior for the scattering process across the visible range, where its intensity is proportional to the fourth power of the laser frequency [63]. The other bands are related to a double or triple resonance process discussed before.

The bands that arise from double or triple resonance may be affected not only by excitation laser energy and defect density, but also by the number of layers as well, where an increasing number of layers will affect the number of allowed processes due to changes in the electronic structure [1, 2]. Although we name the double or triple resonance processes as intervalley and intravalley, we must remember that graphene presents Dirac cones in its electronic structure, not parabolic bands. For the sake of comparison between materials, though, we will stick with this name. The intervalley scattering process [see Fig. 3(b)] occurs when the excited electron is scattered from the conduction band near **K** point to the conduction band near **K**′ point, whereas the intravalley scattering process [see Fig. 3(c)] scatters the electron along the same valley. Once the excited electron is scattered, it can return to its original band through another phonon or a defect, and then it recombines with the hole in the valence band emitting a scattered photon.

The 2D (or G′) band in graphene, appearing between 2600 and 2800 cm^{-1} in Fig. 3(d), is an example of a band originated from the electron–hole intervalley scattering. This process is mediated by two TO phonons (one for the excited electron and one for the hole) around the **K** point in the phonon dispersion and the recombination happens around the **K**′ point [2, 33, 42]. This association is made because the phonon wavevector is around the size of the distance between **K** and **K**′ points, corresponding to the approximate distance between the **Γ** and **K** points [see Fig. 3(b)], which can be mapped to the phonon dispersion. Additionally, the 2D band frequency presents a high dispersion as the excitation laser energy is tuned [around 100 cm^{-1}/eV, see Figs. 3(d) and 3(e)]. The reason for this comes from both the linear electronic dispersion near **K** point of graphene, and the Kohn anomaly, which manifests as strongly dispersive LO branch in the vicinity of the **Γ** and **K** points [73]. Thus, for laser energies close to the linear regime of the electronic dispersion, the intensity of the 2D band is greatly enhanced.

When a graphene sheet presents a significative defect density, a band with approximately half the frequency of the 2D band appears, and it is called D band [36]. The D band is a double resonance process, and its intensity is strongly bound to the defect density [43, 70]. The 2D band, on the other hand, decreases in intensity for increasing defect density [43], which could be argued as a preference for the phonon–defect process instead of the phonon–phonon process of recombination. We mention that as the number of graphene layers increases, the number of intervalley processes increases as well, in accordance

https://doi.org/10.1557/jmr.2019.167 Published online by Cambridge University Press

© Materials Research Society 2019

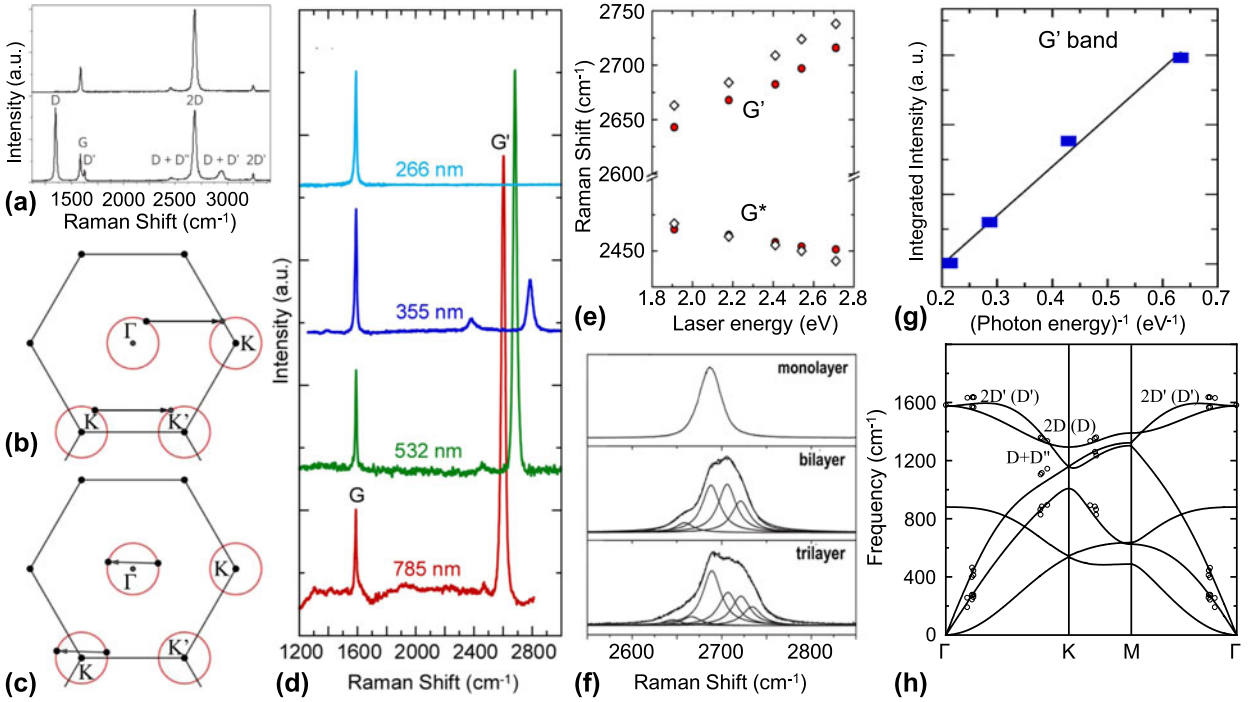


Figure 3: The Raman scattering process in graphene. (a) Raman spectrum of pristine graphene (top) and defective graphene (bottom). Reprinted with permission from Ref. 3. (b) Intervalley and (c) intravalley wave vector scattering processes. (d) Raman spectrum of graphene collected at different excitation wavelengths from NIR to UV. Reprinted with permission from Ref. 63. (e) Frequencies of the 2D and D + D″ (G′ and G*) bands as a function of the laser energy. Reprinted with permission from Ref. 42. (f) Raman spectra of monolayer, bilayer, and trilayer graphene at the same laser energy showing the differences in the observed intervalley processes of the 2D band. Reprinted with permission from Ref. 64. (g) Intensity of the 2D band as a function of the inverse of the laser energy. Reprinted with permission from Ref. 63. (h) Phonon dispersion of single layer graphene with the phonons that participate in the intervalley and intravalley bands, data from Ref. 76.

to the changes in the electronic structure [see Fig. 3(f)] [2, 64]. Also, as the excitation laser energy approaches the UV range, the 2D band intensity considerably decreases (with the first-order process prevailing) such that its intensity is inversely proportional to the excitation laser energy [see Figs. 3(d) and 3(g)] [63]. The D + D″ band, also known in the literature as G* band, is associated with an intervalley scattering involving phonons from TO (D) and LA (D″) branches. Contrarily to the 2D band, the D + D″ presents a negative dispersion due to the behavior of the LA phonon branch around the **K** point [Fig. 3(e)] [2, 42, 74].

The 2D′ band is an example of a phonon–phonon intravalley scattering process [75]. The scattering of the excited electron happens along the **K** cone through the emission of two LO phonons close to the **Γ** point [75]. Analogously, one can also see a D′ band, which is a phonon–defect intravalley scattering [75]. Interestingly, the 2D′ band does not present a strong enhancement of its intensity, showing an intensity smaller than that of a first-order mode. This could be related to the strong interaction between electrons and LO phonons near the **K** point, such that the numerator is also an important factor. Therefore, the electron–phonon interaction is an important factor for the double (or triple) resonance process.

The D′ and 2D′ bands are not very dispersive, i.e., their frequency position does not change much when tuning the excitation laser energy, but they are related to phonon dispersion points where the LO phonon branches are maximum [76].

We comment that combinations of intravalley and intervalley scattering are also possible. For instance, the D + D′ band comes from the scattering of an electron to the **K**′ point mediated by a TO phonon close to the **K** point and then scattered back by a TO phonon close to the **Γ** point. Afterward, electron and hole recombine mediated by a defect [3, 43].

Figure 3(h) shows the phonon dispersion of graphene depicting all the contributions from the double resonance Raman bands associated to their specific points [76]. In summary, the ability to probe phonons away from the **Γ** point in such way that they can be mapped out by their wavevectors is one of the most interesting features of the double Raman resonance bands in layered material.

Before going further, lets analyze all the information gathered so far from the Raman spectra of graphene. The most intense feature in the Raman spectra of monolayer graphene is the 2D band. From the process introduced before, we can infer that not only the triple resonance due to Eq. (2) is important,

https://doi.org/10.1557/jmr.2019.167 Published online by Cambridge University Press

© Materials Research Society 2019

but also a strong interaction between electron and phonons can play a big role for the probability of the process. In fact, the electron–phonon interaction has been found to be twice as strong for LO phonons close to the **K** point than for phonons close to the **Γ** point [35]. This relatively small difference becomes rather strong when we remember that Eq. (2) has a product of two electron–phonon interaction terms that are squared. Thus, an intensity difference of at least eight times can be expected from the 2D and 2D′ bands [35]. Graphene can be considered a semimetal, meaning that it has electronic states available everywhere, except at $E = 0$. Looking at Eq. (2), we realize that there is a term for the electronic transition energy, which is 0 (zero) for graphene. This means that while the linear behavior of the electronic structure is satisfied, graphene is always in resonance. This is true for the NIR and visible spectral regions. This remotes to another important point in the characteristics of the double or triple resonance process, the fact that it is coupled with the position of the electron in the electronic band. Finally, the phonons that participate in the process must conserve momentum, as we have previously mentioned. But, as long as momentum is conserved, any combination of phonons is possible, although the final intensity varies due to the electron–phonon interaction.

Now, we use the guiding principles from graphene and apply them to the analysis of other materials, mostly MoS_2-like TMDs. We emphasize that the knowledge obtained from the analysis of the graphene's Raman spectrum can be extended to other 2D layered materials, although the field has not been thoroughly explored yet and the diverse properties of the material at hand must be considered as well.

TMDs

Few years after the isolation of graphene, semiconducting TMDs monolayers, such as MoS_2 and WS_2, were obtained through the mechanical exfoliation technique and their physical and chemical properties were characterized [77, 78, 79, 80, 81, 82, 83].

TMDs are layered materials composed by a sheet of transition metals (M) sandwiched between two sheets of chalcogens (X) presenting the general chemical formula MX_2. These materials are believed to lead future developments on electronic devices such as optoelectronics [84], valleytronics [85, 86], and wearables [87] in a few years. A diversity of physical properties can be obtained depending on the combination of the transition metal and chalcogen. For instance, it can range from semiconducting (MoS_2, WS_2) to metallic ($NbSe_2$, NbS_2) [88, 89]. Besides, thousands of layered materials are yet to be found [90], showing the great potential of the 2D systems. Despite this great diversity, the study of double resonance Raman scattering is still in progress in these materials. Therefore, in this review, we only focus our analysis on semiconducting MoS_2-like TMDs, discussing the recent advances.

These materials present a characteristic indirect band gap ranging from 1.0 to 1.3 eV when in bulk form [91]. They present strong many-body interactions, such that their optical transitions are governed by excitons, and even at room temperature, their excitonic transition are observed in absorption experiments [92]. Besides, a transition from indirect to direct band gap occurs upon the reduction from bulk to monolayer regime [93]. Due to a strong spin–orbit coupling, a split in the valence band at the **K** point occurs and gives rise to the excitonic transitions named A and B, according to their energy values [92, 94]. Figure 4(a) shows the transition from indirect to direct band gap in the electronic dispersion of MoS_2. The indirect band gap in bulk, which is the phonon-mediated optical transition from the **Γ** to the **Q** point (the midpoint of **Γ**–**K** path), becomes a direct band gap at the **K** point for a monolayer. The phonon dispersion of the MoS_2 class of TMDs is characterized by the presence of nine phonon branches, three acoustic (LA, TA, and ZA) and six optical branches, of irreducible representations A_2', A_1', E′, and E″ at the **Γ** point. Therefore, the expected phonons to participate in the Raman spectrum should be the A_1', E′, and E″ phonons, the last of which is expected to be active only in a right angle configuration.

The nonresonant Raman spectrum of semiconducting TMDs, collected in the backscattering configuration, is mostly restricted to first-order modes, which are known in the literature as the out-of-plane A_1' (A_{1g} for bulk) and the in-plane degenerate E′ (E_{2g} for bulk) mode [8, 9] [see top of Fig. 4(b)]. On the other hand, when the incoming laser energy closely matches the A and B excitonic transitions, new contributions arise in the Raman spectrum of the material [see bottom of Fig. 4(b)]. These new features can be associated with the intervalley scattering mediated by acoustic phonons [11, 47, 48, 50, 52, 53, 58, 95]. For instance, in MoS_2, two bands are mainly observed in its resonant Raman spectrum: a band at approximately 420 cm^{-1} commonly known in the literature as "b" band [50, 52, 53], and a broad and asymmetric band at approximately 460 cm^{-1}, which is related to two LA phonons [Fig. 4(c)] [44, 50, 54, 57, 96, 97]. A detailed discussion about the origin of these bands will be presented later on.

Before that, to understand the physical meaning of the double resonance bands involving the acoustic phonons, it is necessary to separate the simple second-order Raman process and double resonance process that overlap in a resonant Raman spectrum of TMDs.

Second-order bands are present in the Raman spectrum of several materials, and their main characteristic is the fact that they are the reflection of the phonon density of states of the

https://doi.org/10.1557/jmr.2019.167 Published online by Cambridge University Press

© Materials Research Society 2019

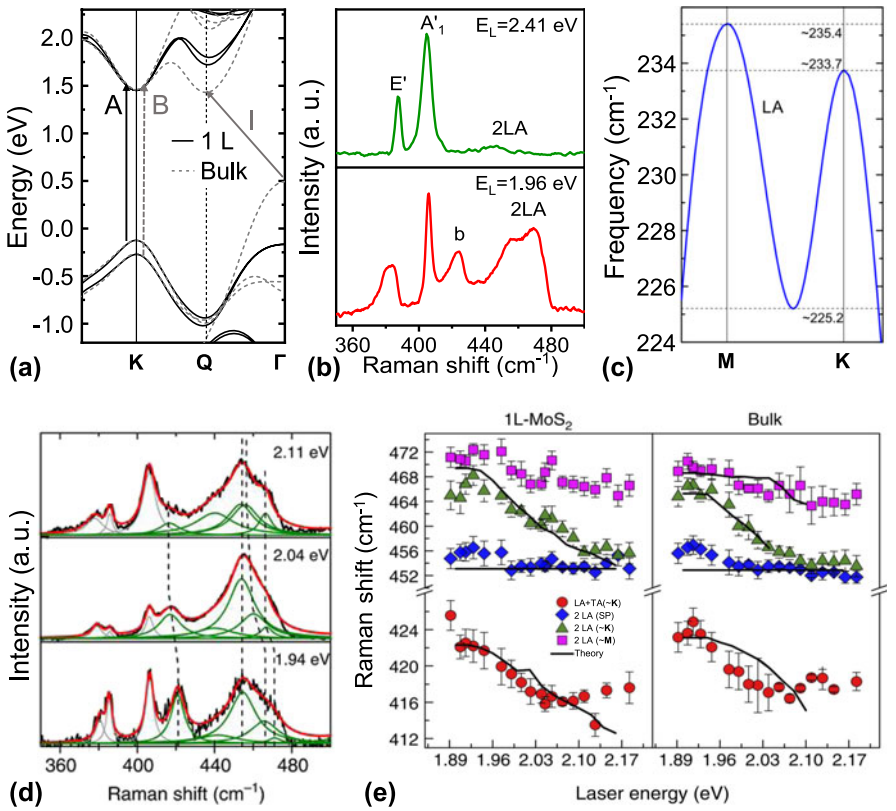


Figure 4: The Raman scattering process in MoS_2 transition–metal dichalcogenide. (a) Electronic band structure with a close-up of the **K**, **Q**, and **Γ** points showing the indirect to direct band gap transitions from bulk to monolayer MoS_2. The A and B excitons are highlighted by vertical arrows. (b) Raman spectra of monolayer MoS_2 off-resonance (top) and on-resonance (bottom) with the excitonic transition. (c) The LA phonon branch dispersion close to the **K** and **M** points. Reprinted with permission from Ref. 50 (from supplementary information). Raman spectra of monolayer MoS_2 off-resonance (top) and on-resonance (bottom) with the excitonic transition. (d) Raman spectra of monolayer MoS_2 collected at different laser energies across the A and B excitons. (e) Frequencies of the LA + TA(∼**K**) band and the components of the 2LA band: singularity, 2LA(∼**K**) and 2LA(∼**M**) as a function of the laser energy. (c–e) Reprinted with permission from Ref. 50.

material with double the original frequency. This means that their position does not change with the laser energy in contrast to double resonance bands. A recent theoretical work for silicon has shown that the Raman intensity of the second-order bands are highly affected by the many-body effects that come into play [98]. Thus, the second-order bands are greatly enhanced when the laser energy matches the electronic transition of the material. The difference between second-order and double resonance bands, however, can be observed when several laser lines are used to measure the Raman spectra close to the electronic transition, revealing the pattern where the dispersion of the bands can be observed.

Several works have reported the study of the double resonance process in TMDs [47, 48, 50, 63, 95, 99, 100]. These reports show that the double resonance bands observed in TMDs are mostly due to intervalley scattering. As it can be seen in Fig. 4(b), the peak at around 460 cm^{-1} associated with a double resonance band is asymmetric and its shape strongly depends on the excitation laser energy and number of layers, thus more than one process may be participating in this band [3, 35, 43].

The first observation of a double resonance band in bulk MoS_2 was reported by Sekine et al. in 1984, where the authors observed a dispersive Raman feature named as "*b*" band located at approximately 420 cm^{-1} [53]. This feature presented a high dispersion with the laser energy close to the *A* and *B* excitons. To explain such high dispersion, the authors proposed a mechanism considering a two-phonon scattering of one quasiacoustic phonon and an optical phonon, parallel to the *c* axis of the crystal [53]. Similar mechanism was later proposed for the "*b*" band by taking into account the explanation of the anti-Stokes process [58]. However, these models were not compatible with the observed resonant Raman spectrum of a monolayer MoS_2, which had a similar band but lacked a quasiacoustic phonon branch. Additionally, Chen et al. and later Stacy et al. reported another band in the resonant Raman spectrum of bulk MoS_2 located at 460 cm^{-1}, the intensity and shape of which strongly change as the excitation energy is tuned [54, 96]. This band has been attributed to a combination of two LA phonons at the **M** point. Henceforth, few other works have tried to associate this band to different combinations of phonons [97, 101], but none of these works presented a satisfactory explanation of the origin of this band.

https://doi.org/10.1557/jmr.2019.167 Published online by Cambridge University Press

© Materials Research Society 2019

Using what we saw for graphene, we can start to propose a better explanation based not only on the rules observed, but also on other known features of the TMDs, such as their phonon dispersion and electronic structure. Considering an electron–electron two-phonon intervalley scattering from **K** to **K′** in the conduction band of MoS_2, we can ask which phonons could participate in such process. Since, from graphene, the phonons must present strong interaction with the electron, we can suppose that the phonons involved in the intervalley scattering must be acoustic phonons, due to the strong correlation between the excitonic transitions in MoS_2 and the acoustic phonons [102, 103, 104, 105]. This is especially true since the phonon energy that we observe experimentally is very close to double the frequencies of the LA phonons in the **K** and **M** points [Fig. 4(c)]. This means that there could be a double resonance process occurring that actually involves those phonons.

Using the train of thought above, it was proposed in Ref. 50 a model based on theoretical and experimental results to explain the origin of both *b* and 2LA bands [see Figs. 4(d) and 4(e)] [50]. The authors have performed resonant Raman measurements across the *A* and *B* excitons levels on monolayer and bulk MoS_2. By tracking the behavior on frequency and intensity of the *b* and 2LA Raman bands and calculating the on-resonance electrons and phonons that participate in the scattering process, it was shown that the *b* band could be associated with a combination of phonons from the LA and TA phonon branches around the **K** point due to a double resonance electron–electron intervalley scattering process, i.e., LA + TA(∼**K**). This process is analogous to the D + D″ band in graphene, where two different phonons with the same wavevector participate in the electron scattering process.

As for the 2LA band, the authors deconvoluted this broad band by a set of Lorentzian peaks and showed that it is composed of at least three components that can be highlighted: two double resonance bands and one second-order band [see Fig. 4(d)]. The two double resonance features are associated with the electron scattering by two LA phonons at the proximities of the **K** and **M** points, which were assigned as 2LA(∼**K**) and 2LA(∼**M**) located around 460 cm^{-1} and 470 cm^{-1}, respectively. The second-order mode is located at 452 cm^{-1} related to a singularity in the phonon density of states present due to a saddle point in the LA phonon branch between the **K** and **M** points. The above assignment was proposed due to the analysis of the observed difference in intensity band from bulk to monolayer, where the 2LA(∼**M**) phonon has higher contribution in few layers and bulk than in monolayer since this process is mediated by the indirect band gap [49, 56].

The frequency position of 2LA(∼**K**) and 2LA(∼**M**) decreases as the laser energy increases, this negative dispersive behavior is contrary to the observed for the 2D band of graphene but resembles the behavior of the D + D″ band. The negative dispersion is a result of the wavevectors that are accessed by the excited electron as it is scattered from **K** to **K′** points. The frequency of the LA branch decreases for wavevectors further from the **K** or **M** points [Fig. 4(b)], which will both contribute to the double resonance bands, hence resulting in a negative dispersion. To this date, the dispersive behavior in TMDs has only been reported for semiconducting MoS_2 [50].

Some works have reported the study of the Raman spectrum of MoS_2 in the UV range to gain further information about other high-order resonance processes. Sun et al. observed that the Raman spectrum of MoS_2 in bulk, monolayer, bilayer and trilayer samples, collected with an excitation energy of 3.81 eV [see Fig. 5(a)], presents three strong bands in the 750 to 840 cm^{-1} spectral range, which were associated to combinations of E_{2g} and A_{1g} modes [11]. It was proposed that these bands are originated by a triply resonant hole–hole Raman scattering process, where the hole would be scattered from the bottom of the spin–orbit split at the valence band to the top valence band and later recombines with the electron [see Fig. 5(b)]. Liu et al. have observed the presence of several new peaks between 560 and 820 cm^{-1} spectral range in the Raman spectrum of monolayer MoS_2 collected with a 3.50 eV laser energy [47] [see Fig. 5(c)]. The observed bands were related to intervalley scatterings between points at half way from **Γ** to **K**, where the absorption of this laser energy is strongest according to the theoretical calculations reported [see inset of Figs. 5(c) and 5(d)]. The observed phonons were associated with their correct wavevectors in the phonon dispersion [see Fig. 5(e)] [47]. A similar study has also been done recently for WS_2 [100].

Guo et al. have investigated the Raman spectra of $MoTe_2$ using three laser lines of energy 1.58, 1.96, and 2.33 eV [48] [see Fig. 5(f)]. A set of new Raman bands was observed and associated with intervalley scattering between the proximities of **M** point [see Fig. 5(g)]. The contribution of each laser energy to the observed bands was calculated and connected to their correct wavevectors [see Fig. 5(h)]. Although these works are promising, they are still in infancy because further probe by tuning the excitation laser energy and number of layers (that helps to unveil the Raman scattering process) needs to the performed for the 2D family.

Most of the works in the literature investigate the Raman spectrum of TMDs by tuning the excitation laser energy to probe the resonance effects. However, a closer inspection at the Raman intensity equations [see Eqs. (1) and (2)] can provide more insightful thoughts regarding the Raman scattering process. The intensity can be tuned not only by changing the excitation laser energy, but also by changes in the excitonic transition energy itself. Such changes in the excitonic transition

https://doi.org/10.1557/jmr.2019.167 Published online by Cambridge University Press

© Materials Research Society 2019

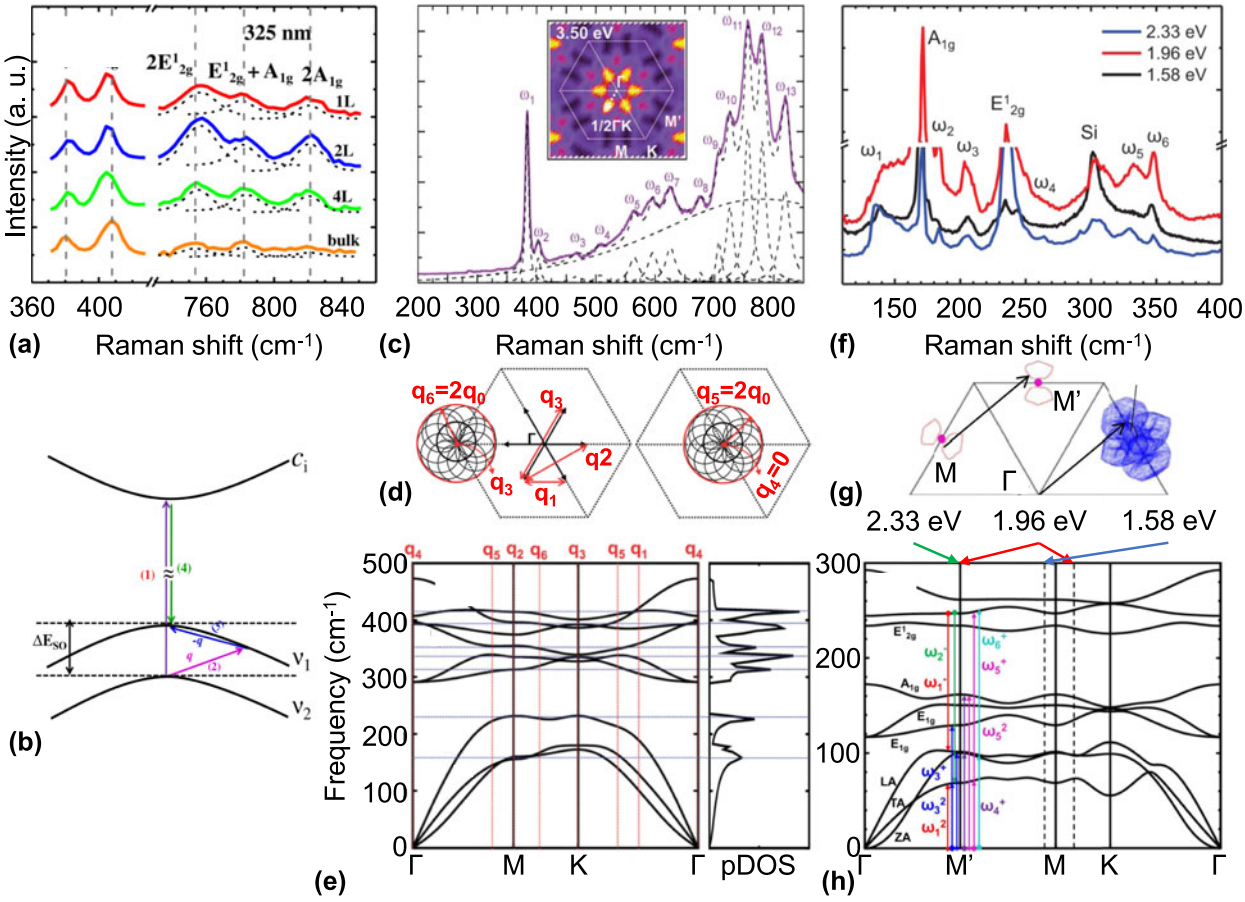


Figure 5: Double resonance Raman bands above the excitonic transitions. (a) Raman spectrum of monolayer, bilayer, trilayer, and bulk MoS_2 collected with a UV laser of 3.81 eV. (b) Proposed triple resonance process. (a) and (b) Reprinted with permission from Ref. 11. (c) Raman spectrum of monolayer MoS_2 collected with a UV laser of 3.50 eV. The inset shows the calculated absorption probability for this laser energy. (d) Proposed scattering process near the **Γ** point responsible for the observed Raman bands in (c). (e) Complete phonon dispersion of MoS_2 with the different contributions of the double resonance bands in (c) and (d) ascribed to their respective points in the Brillouin zone. (c–e) Reprinted with permission from Ref. 47. (f) Raman spectra of monolayer $MoTe_2$ collected for three laser energies. (g) Proposed electron scattering near the **M** points for a laser energy of 1.96 eV. (h) Phonon dispersion of $MoTe_2$ with observed contributions to the Raman spectra from the three laser energies ascribed to their respective points in the Brillouin zone. (f–h) Reprinted with permission from Ref. 48.

energy can be achieved, for example, by in situ variation of the sample's temperature or pressure. For instance, tuning the exciton energy for bulk MoS_2, either by temperature or pressure changes, affects the double resonance processes just like if the excitation laser energy is being tuned [58]. Recent works on monolayer MoS_2 have shown that under temperature variation the frequency position of the double resonance LA + TA(~**K**) band (i.e., the *b* band) disperses by a rate of $(\Delta\omega/\Delta T)_b = 0.035\ \mathrm{cm}^{-1}/\mathrm{K}$, while the first-order A'_1 mode disperses $(\Delta\omega/\Delta T)_{A'_1} = 0.008\ \mathrm{cm}^{-1}/\mathrm{K}$ [52]. This represents a dispersive rate ratio of around 4.4 times between the double resonance and first-order bands, which is a good indicative of changes in the excitonic effects leading to the strongly dispersive behavior of the *b* band.

We end this section reminding that the strong enhancement of the double resonance Raman bands in MoS_2-like TMDs comes from the resonance with the excitonic transitions. Therefore, out of resonance, the Raman bands should show little intensity, and would barely be observable, which is the case shown in Fig. 4(b), where we compare the spectra of monolayer MoS_2 at a laser far from resonance (2.41 eV) and a laser very close to resonance with the *A* exciton (1.96 eV). These are important considerations because in the next section we will discuss defects in 2D systems, and resonance with the electronic levels of the material is fundamental to measure the contributions of defect-induced bands to the Raman spectra.

Probing defects in 2D systems

Controlling defects in materials is of utmost importance for the development of technology due to its role on tuning the doping concentration or carrier types, reducing contact resistance in electronic devices, and improving the responsivity, speed, and operation wavelength of photodetectors in novel optoelectronic

https://doi.org/10.1557/jmr.2019.167 Published online by Cambridge University Press

© Materials Research Society 2019

devices, such as photodetectors and LEDs [60]. Therefore, a quantitative way to control the density of defects in 2D materials is a key ingredient to the development of 2D materials technology. In this aspect, Raman spectroscopy is a simple and nondestructive tool that allows the characterization and quantification of defects in 2D materials.

Defects can be generated either during (in situ defects) or after (ex situ defects) the synthesis process [59], where the latter is extended to exfoliated samples. Several kinds of in situ defects can be generated such as vacancies of chalcogens and metals (usually accompanied with their bonds) in TMDs, antisites, grain boundaries, edges, and line defects [106]. These in situ defects are not controllable. However, ex situ defects can be created in a controllable way due to the improvement of the defect engineering in 2D materials. For example, electron beam irradiation [107, 108] and ion (Mn^+ and Ar^+) bombardment [62, 109] have been used to create chalcogen vacancies in TMDs, where the distance among vacancies can be controlled by the beam dosage. The same approach can also be used to create MoS_2 nanocrystallites [110]. Additionally, the introduction of vacancies by electron irradiation can be followed by doping [111]. Indeed, oxygen substitution of chalcogenides may occur in normal ambient conditions despite the slow rate of the reaction and difficulties to be controlled [112]. However, oxygen passivation of chalcogen vacancies using laser annealing has been performed in WSe_2 as an alternative, improving its conductivity and photoconductivity [112]. Besides, doping by potassium [113] was achieved before theoretical studies for alkali metals (Li, K, and Cs) doping in TMDs [114] while lithium doping has been recently done [115]. All this shortly highlights the importance to probe defects in 2D materials. Hence, in the following, we briefly comment the study of defects in graphene and semiconducting TMDs by Raman spectroscopy, which allows to probe and understand the defects scattering in 2D systems.

Defects in graphene

Defects allow the appearance of new features in the Raman spectrum of graphene considering that the defect density increases up to a certain threshold, as shown in Fig. 6(a). The defect density is related to the fluence of ions into the samples (in order of 10^{11} to 10^{14}) [116], but most works in the literature quantify the amounts of defects by the average defect distance (L_D), given by $L_D = 1/\sqrt{\eta}$, where η is the defect density [3, 35, 43, 62, 70, 71, 72]. The reason for this choice is because it provides a direct correlation between defects and their effects on the Raman spectrum. The Raman spectrum of a defective graphene sample presents three new features assigned as D, D′, and D + D′ bands, as it is shown in [see Fig. 6(a)] [43]. These new Raman bands are the result of intervalley, intravalley, and combination of both processes where the conservation of momentum is preserved by the presence of a defect.

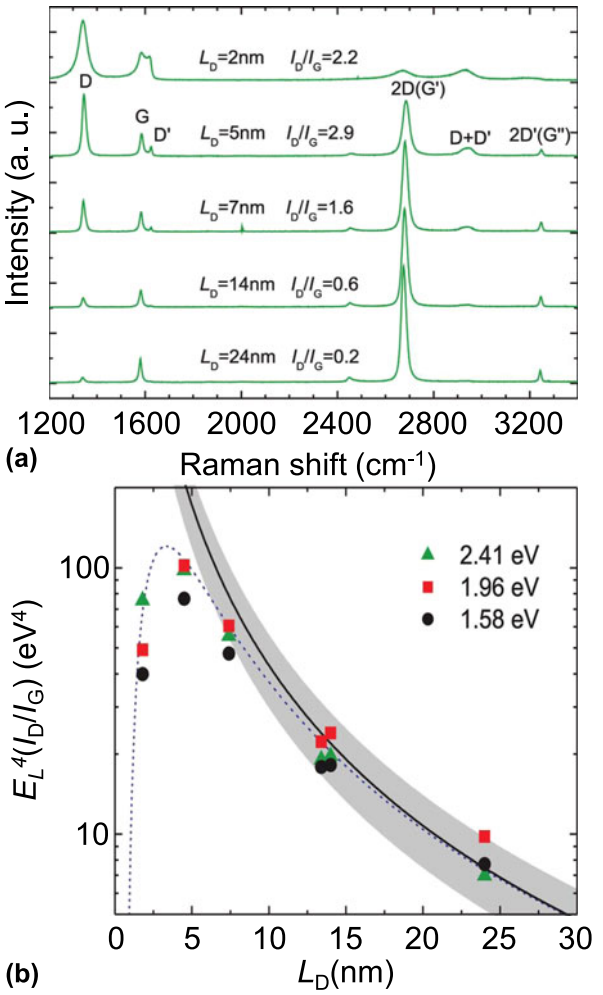


Figure 6: One-phonon defect Raman spectrum of a defective graphene. (a) Raman spectrum of monolayer graphene for different values of interdefect distance (L_D) collected with a 2.41 eV laser. (b) Intensity ratio of D to G band multiplied by the fourth power of the laser energy as a function of interdefect distance. Reprinted with permission from Ref. 43.

In Fig. 6(a), we can notice that the D band is the most intense one of the defective Raman features in graphene. It has half the frequency of the 2D band and shows a dispersive behavior as the excitation laser energy is tuned [43]. Additionally, the D band also depends on the average defect distance, L_D, because its intensity increases as the L_D value decreases [see Fig. 6(a)]. Notice that D band intensity can even surpass the G band intensity. The intensity ratio of both bands (I_D/I_G) provide a route to characterize the sample quality [see Fig. 6(a)] [43]. The relationship between of the I_D/I_G intensity ratio can be expressed as a function of L_D given by [43, 70]

$$\frac{I_D}{I_G} = C_A \frac{(r_A^2 - r_S^2)}{(r_A^2 - 2r_S^2)} \left[\exp\left(-\pi \frac{r_S^2}{L_D}\right) - \exp\left(-\pi \frac{r_A^2}{L_D} + \pi \frac{r_S^2}{L_D}\right) \right], \quad (3)$$

where r_A and r_S are length scales related to either the regions that contribute to the scattering of the electron to form the D

https://doi.org/10.1557/jmr.2019.167 Published online by Cambridge University Press

© Materials Research Society 2019

band or to the disorder caused by defect formation. C_A is a weight parameter that depends on the laser energy. By Eq. (3), it is possible to observe the behavior of the intensity of the D band as a function of both laser energy and defect length. A laser-independent relationship can also be obtained by multiplying the left side of Eq. (3) by E_L^4, as it is shown in Fig. 6(b) [43]. This new expression allows to monitor and control the defect density in graphene for its applications, independently of the laser line used.

It is worthy of note that after the threshold of the defect amounts is reached, i.e., the L_D is considerably small, there is a change in the crystallinity of the sample becoming increasingly rich in sp^3 amorphous carbon [3, 43]. At this point, several changes in the Raman spectrum are observed, including broadening and asymmetry of the bands, shifts in frequency of the first-order modes, among others [3, 43, 70, 71].

Defects in TMDs

As in graphene, the presence of defects can also impact the Raman spectrum of TMDs. However, the impact in TMDs is far less sensitive than those observed for graphene. For graphene, the D band can be directly observed in the Raman spectrum with L_D up to 25 nm [43, 70]. Graphene is always in resonance on the NIR and most of the visible range; thus, most of the double resonance processes involving defects are fairly strong, in special when the L_D is low enough that we can expect a big enhancement of the defect-induced bands. For semiconducting TMDs, unless the sample is resonantly excited [49, 50] across the excitonic transitions, the disorder-induced bands can be barely observed. These bands are associated to the acoustic branches and can only be observed when a small L_D is reached, meaning a high defect density [49, 62, 110].

As the size of the analyzed crystal decreases, the selection rule for zone center phonons can be dropped. Therefore, a new domain size where L_D needs to be accounted for must be considered for confinement effects. The uncertainty principle states that the momentum uncertainty of the electron will be proportional to $(L_D)^{-1}$, which will involve phonons away from the $\mathbf{\Gamma}$ point. As a result, the shape of the Raman bands changes from a regular Lorentzian, related to a forced, damped harmonic oscillator, to a broader and asymmetric shape. This new shape can be described by a weighted sum over all the phonons in the Brillouin zone within a Gaussian distribution related to the mean defect distance [62, 110],

$$I(\omega) = \int_{BZ} \frac{\exp\left(-(qL_D/2\alpha)^2\right)}{\left(\omega - \omega_{Ph}(\mathbf{q})\right)^2 + (\gamma/2)} d\mathbf{q} \quad . \qquad (4)$$

The α parameter is a constant that relates the mean defect distance to the phonon confinement length by defects or microcrystalline size, $\omega_{Ph}(\mathbf{q})$ is the phonon branch frequency, and γ is a broadening factor that increases as the defect mean distance decreases. Notice that as L_D increases to infinity (for pristine samples), the usual Raman line shape of a Lorentzian is recovered. This model can be used to describe the disorder in several systems other than TMDs, as it has already been used for graphene and graphite [71, 116], silicon [117, 118], and GaAs [119].

The first-order bands are also affected by increasing the disorder density. The effects observed are frequency shifts and an increased broadening in contrast to pristine samples. Figure 7(a) shows the nonresonant Raman spectrum of semiconducting MoS_2 monolayers with different L_D. We can clearly observe how the first-order E′ and A_1' modes are altered. A new peak associated with the defect-induced LA mode is also observed [56, 57]. This defect-induced peak is located at around 230 cm^{-1}, half the frequency of the 2LA band [56, 57].

The shift and increased broadening observed in the Raman spectrum of MoS_2 are related to a smaller phonon correlation length L_C, which is a measure of the phonon confinement by defects or microcrystallite size and it is proportional to the L_D parameter. Similar to graphene, the intensity ratio of the disorder-induced LA band and the first-order modes A_1' and E′, i.e., $I_{LA}/I_{A1'}$ and $I_{LA}/I_{E'}$, can provide a way to quantify the amounts of defects [see Fig. 7(b)] [62]. This has also been observed by Li-doped MoS_2 monolayer samples, where the LA band is rapidly intensified for increasing lithium exposure time [115].

One important remark is that the disorder-induced LA band is composed by at least three components: LA(~**K**), LA(~**M**), and a band associated to a singularity from the phonon density of states [Fig. 7(c)]. The peak position of these Raman bands presents half the frequency of the bands composing the 2LA band. Therefore, the LA(~**K**) and LA(~**M**) modes also present a dispersive behavior with the excitation laser energy, following a similar trend as the dispersive two-phonon features composing the 2LA band [50]. The observation of these three components in the defect-induced LA band, and the fact that these components present half of the calculated dispersion of the 2LA(~**K**) and 2LA(~**M**) bands, further strengthens the intervalley double resonance scattering model claim proposed in Ref. [50] for semiconducting MoS_2 [see Fig. 7(d)].

To our knowledge, such detailed analysis of the double resonance process in defective TMDs sample was only explored for the MoS_2. Recently, however, it was reported the presence of two new bands in the tip-enhanced Raman spectrum of a defective WS_2 sample, called D and D′ [120]. The appearance of these new bands was related to an increased number of sulfur vacancies, and the D band was associated with the A_1' phonon branch. The D′ band was associated with the infrared-

https://doi.org/10.1557/jmr.2019.167 Published online by Cambridge University Press

© Materials Research Society 2019

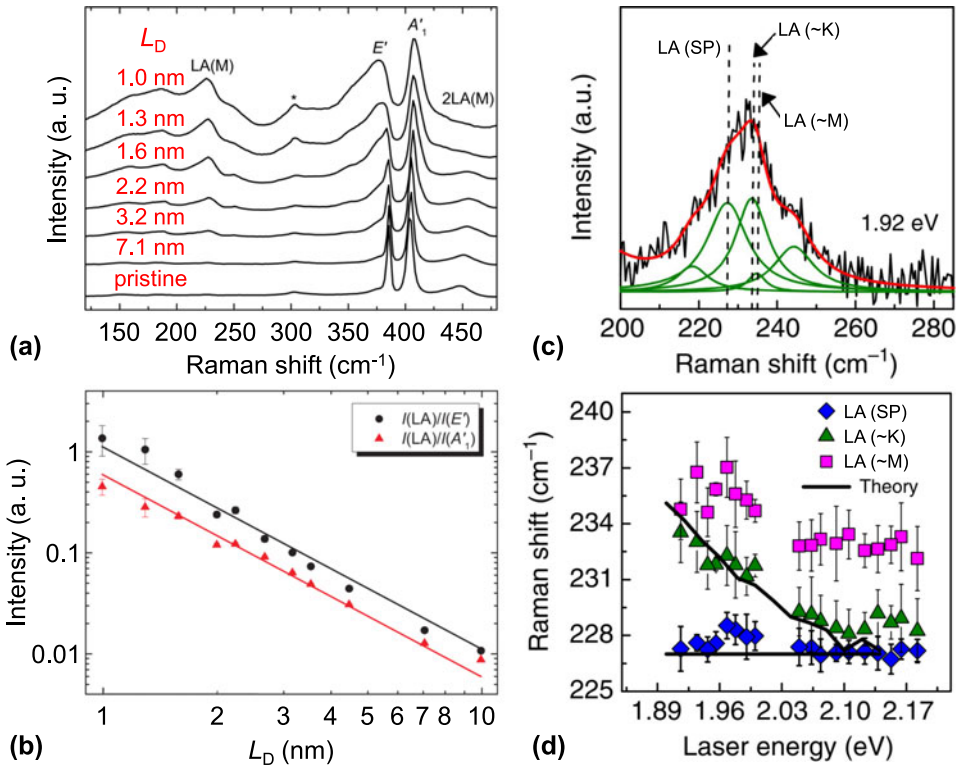


Figure 7: Phonon–defect Raman spectrum of monolayer MoS_2. (a) Raman spectrum of monolayer MoS_2 for different values of interdefect distances collected with a 2.41 eV laser. (b) Intensity ratio between LA band and the A_1' and E′ bands. The observed line is a fit with a curve proportional to $(L_D)^{-2}$. Reprinted with permission from Ref. 62. (c) Deconvolution of the defective LA band in monolayer MoS_2. (d) Frequencies of the LA band components in (c) as a function of the laser energy. Reprinted with permission from Ref. 50.

active A_2'' [120]. This study, however, was a single laser line study of the Raman spectrum of WS_2 and the only one so far about this material where defect-induced bands appear.

There are a few other works that have measured the contribution of the defect-induced bands in the Raman spectrum of semiconducting TMDs [49, 62, 110]. These works reported changes to the observed spectra related to different wavevectors accessed by the high density of defects present in the samples. More importantly, they have observed mainly changes around the first-order modes, which means that the main contributions are related to optical phonons.

Conclusion and perspectives

In this review, we have discussed the double resonance Raman bands in 2D materials. We have focused on the state-of-the-art 2D materials: graphene and semiconducting MoS_2. We have explained the most pronounced bands that arise from the electron–electron, electron–hole, and hole–hole intravalley and intervalley scattering process. These scattering processes allow phonons at the Brillouin zone edge to participate in the scattering where the momentum conversation is preserved by a two-phonon or one-phonon defect process. Such processes allow the observation of the D, D′, D + D″, 2D, and 2D′ Raman bands of graphene mediated by phonons at the vicinity of the **K** and **Γ** points, whereas the electron–electron intervalley scattering allows the observation of the LA, *b*, and 2LA Raman bands in MoS_2 mediated by phonons near the **K** and **M** Brillouin zone edge points.

There are other few works on the study of the double resonance Raman bands in other TMDs providing insights on the scattering process. However, up to this date, the detailed analysis of the double resonance Raman process has been described only for the semiconducting MoS_2. The latter has shown that a more in-depth resonant Raman study for the other materials is still needed to properly observe the possible double resonance contributions in the Raman spectrum of the other TMDs. In particular, the study of other classes of TMDs is lacking, especially those with high anisotropic optical properties such as ReS_2 and $ReSe_2$ [121, 122]. It could be very interesting to observe the possible behavior of double resonance bands of these materials, even though their optical transitions are very far from the most common lasers used in the collection of the Raman spectrum at 1.3–1.5 eV [121, 122].

A recent study of bulk black phosphorous has observed the presence of several small intensity bands, which were ascribed

https://doi.org/10.1557/jmr.2019.167 Published online by Cambridge University Press

© Materials Research Society 2019

to two-phonon bands [123]. The intensity of these bands reaches a maximum close to a laser energy of 2.4 eV, indicating a presence of an electronic transition [123]. It remains to be seen whether the same effect will be visible in single layer or even few layers samples. One study has observed the presence of new bands in defective monolayer and few layers of black phosphorus, which were assigned to phonon–defect intravalley processes [124]. Although, in comparison with graphene, more works should be done to assess some other possible effects that could be present.

The emerging of new 2D materials shows that the field on double resonant Raman process is still in progress and more work needs to be done for a deeper understanding of the underlying physics of the double resonance process in other materials. The double resonance Raman mechanism provides important information for the understanding of the photophysics of 2D materials, the quantification of defects, and to describe the intervalley and intravalley scattering of electrons essential for the development of the spintronics and valleytronics.

Acknowledgments

The authors acknowledge the final support from the Instituto Nacional de Ciência e Tecnologia (INCT) em Nanomateriais de Carbono (Federative Republic of Brazil), Coordenação de Aperfeiçoamento de Pessoal de Nível Superior (CAPES, Federative Republic of Brazil), Conselho Nacional de Desenvolvimento Científico e Tecnológico (CNPq, Federative Republic of Brazil), and Fundação de Amparo à Pesquisa do Estado de Minas Gerais (FAPEMIG, Federative Republic of Brazil).

References

1. **A.C. Ferrari, J.C. Meyer, V. Scardaci, C. Casiraghi, M. Lazzeri, F. Mauri, S. Piscanec, D. Jiang, K.S. Novoselov, S. Roth, and A.K. Geim**: Raman spectrum of graphene and graphene layers. *Phys. Rev. Lett.* **97**, 1 (2006).
2. **L.M.M. Malard, M.A.A. Pimenta, G. Dresselhaus, and M.S.S. Dresselhaus**: Raman spectroscopy in graphene. *Phys. Rep.* **473**, 51 (2009).
3. **A.C. Ferrari and D.M. Basko**: Raman spectroscopy as a versatile tool for studying the properties of graphene. *Nat. Nanotechnol.* **8**, 235 (2013).
4. **H.B. Ribeiro, M.A. Pimenta, and C.J.S. de Matos**: Raman spectroscopy in black phosphorus. *J. Raman Spectrosc.* **49**, 76 (2018).
5. **S. Reich, A.C. Ferrari, R. Arenal, A. Loiseau, I. Bello, and J. Robertson**: Resonant Raman scattering in cubic and hexagonal boron nitride. *Phys. Rev. B* **71**, 205201 (2005).
6. **Q. Cai, D. Scullion, A. Falin, K. Watanabe, T. Taniguchi, Y. Chen, E.J.G. Santos, and L.H. Li**: Raman signature and phonon dispersion of atomically thin boron nitride. *Nanoscale* **9**, 3059 (2017).
7. **C. Attaccalite, L. Wirtz, A. Marini, and A. Rubio**: Efficient Gate-tunable light-emitting device made of defective boron nitride nanotubes: from ultraviolet to the visible. *Sci. Rep.* **3**, 2698 (2013).
8. **M.A. Pimenta, E. del Corro, B.R. Carvalho, C. Fantini, and L.M. Malard**: Comparative study of Raman spectroscopy in graphene and MoS_2-type transition metal dichalcogenides. *Acc. Chem. Res.* **48**, 41 (2015).
9. **R. Saito, Y. Tatsumi, S. Huang, X. Ling, and M.S. Dresselhaus**: Raman spectroscopy of transition metal dichalcogenides. *J. Phys.: Condens. Matter* **28**, 353002 (2016).
10. **C.H. Lui, Z. Ye, C. Ji, K-C. Chiu, C-T. Chou, T.I. Andersen, C. Means-Shively, H. Anderson, J-M. Wu, T. Kidd, Y-H. Lee, and R. He**: Observation of interlayer phonon modes in van der Waals heterostructures. *Phys. Rev. B* **91**, 165403 (2015).
11. **L. Sun, J. Yan, D. Zhan, L. Liu, H. Hu, H. Li, B.K. Tay, J-L.L. Kuo, C-C.C. Huang, D.W. Hewak, P.S. Lee, and Z.X. Shen**: Spin–orbit splitting in single-layer MoS_2 revealed by triply resonant Raman scattering. *Phys. Rev. Lett.* **111**, 126801 (2013).
12. **B.R. Carvalho, L.M. Malard, J.M. Alves, C. Fantini, and M.A. Pimenta**: Symmetry–dependent exciton-phonon coupling in 2D and bulk MoS_2 observed by resonance Raman scattering. *Phys. Rev. Lett.* **114**, 136403 (2015).
13. **E. del Corro, A. Botello-Méndez, Y. Gillet, A.L. Elias, H. Terrones, S. Feng, C. Fantini, D. Rhodes, N. Pradhan, L. Balicas, X. Gonze, J-C. Charlier, M. Terrones, and M.A. Pimenta**: Atypical exciton–phonon interactions in WS_2 and WSe_2 monolayers revealed by resonance Raman spectroscopy. *Nano Lett.* **16**, 2363 (2016).
14. **P. Soubelet, A.E. Bruchhausen, A. Fainstein, K. Nogajewski, and C. Faugeras**: Resonance effects in the Raman scattering of monolayer and few-layer $MoSe_2$. *Phys. Rev. B* **93**, 155407 (2016).
15. **C. Lee, H. Yan, L.E. Brus, T.F. Heinz, J. Hone, and S. Ryu**: Anomalous lattice vibrations of single- and few-layer MoS_2. *ACS Nano* **4**, 2695 (2010).
16. **H. Li, Q. Zhang, C.C.R. Yap, B.K. Tay, T.H.T. Edwin, A. Olivier, and D. Baillargeat**: From bulk to monolayer MoS_2: Evolution of Raman scattering. *Adv. Funct. Mater.* **22**, 1385 (2012).
17. **X. Zhang, X-F. Qiao, W. Shi, J-B. Wu, D-S. Jiang, and P-H. Tan**: Phonon and Raman scattering of two-dimensional transition metal dichalcogenides from monolayer, multilayer to bulk material. *Chem. Soc. Rev.* **44**, 2757 (2015).
18. **A. Molina-Sánchez, K. Hummer, and L. Wirtz**: Vibrational and optical properties of MoS_2: From monolayer to bulk. *Surf. Sci. Rep.* **70**, 554 (2015).

https://doi.org/10.1557/jmr.2019.167 Published online by Cambridge University Press

© Materials Research Society 2019

19. **A.A. Puretzky, L. Liang, X. Li, K. Xiao, K. Wang, M. Mahjouri-Samani, L. Basile, J.C. Idrobo, B.G. Sumpter, V. Meunier, and D.B. Geohegan**: Low-frequency Raman fingerprints of two–dimensional metal dichalcogenide layer stacking configurations. *ACS Nano* **9**, 6333 (2015).
20. **K. Kim, J.U. Lee, D. Nam, and H. Cheong**: Davydov splitting and excitonic resonance effects in Raman spectra of few-layer $MoSe_2$. *ACS Nano* **10**, 8113 (2016).
21. **L. Du, M. Liao, J. Tang, Q. Zhang, H. Yu, R. Yang, K. Watanabe, T. Taniguchi, D. Shi, Q. Zhang, and G. Zhang**: Strongly enhanced exciton-phonon coupling in two-dimensional WSe_2. *Phys. Rev. B* **97**, 235145 (2018).
22. **I. Bilgin, A.S. Raeliarijaona, M.C. Lucking, S.C. Hodge, A.D. Mohite, A. de Luna Bugallo, H. Terrones, and S. Kar**: Resonant Raman and exciton coupling in high-quality single crystals of atomically thin molybdenum diselenide grown by vapor–phase chalcogenization. *ACS Nano* **12**, 740 (2018).
23. **M-H. Chiu, M-Y. Li, W. Zhang, W-T. Hsu, W-H. Chang, M. Terrones, H. Terrones, and L-J. Li**: Spectroscopic signatures for interlayer coupling in MoS_2–WSe_2 van der Waals stacking. *ACS Nano* **8**, 9649 (2014).
24. **G.W. Shim, K. Yoo, S-B. Seo, J. Shin, D.Y. Jung, I-S. Kang, C.W. Ahn, B.J. Cho, and S-Y. Choi**: Large–area single–layer $MoSe_2$ and its van der Waals heterostructures. *ACS Nano* **8**, 6655 (2014).
25. **Y. Gong, S. Lei, G. Ye, B. Li, Y. He, K. Keyshar, X. Zhang, Q. Wang, J. Lou, Z. Liu, R. Vajtai, W. Zhou, and P.M. Ajayan**: Two–step growth of two-dimensional WSe_2/$MoSe_2$ heterostructures. *Nano Lett.* **15**, 6135 (2015).
26. **K. Zhang, T. Zhang, G. Cheng, T. Li, S. Wang, W. Wei, X. Zhou, W. Yu, Y. Sun, P. Wang, D. Zhang, C. Zeng, X. Wang, W. Hu, H.J. Fan, G. Shen, X. Chen, X. Duan, K. Chang, and N. Dai**: Interlayer transition and infrared photodetection in atomically thin type-II $MoTe_2$/MoS_2 van der Waals heterostructures. *ACS Nano* **10**, 3852 (2016).
27. **G.S.N. Eliel, M.V.O. Moutinho, A.C. Gadelha, A. Righi, L.C. Campos, H.B. Ribeiro, P-W. Chiu, K. Watanabe, T. Taniguchi, P. Puech, M. Paillet, T. Michel, P. Venezuela, and M.A. Pimenta**: Intralayer and interlayer electron–phonon interactions in twisted graphene heterostructures. *Nat. Commun.* **9**, 1221 (2018).
28. **M-L. Lin, Q-H. Tan, J-B. Wu, X-S. Chen, J-H. Wang, Y-H. Pan, X. Zhang, X. Cong, J. Zhang, W. Ji, P-A. Hu, K-H. Liu, and P-H. Tan**: Moiré phonons in twisted bilayer MoS_2. *ACS Nano* **12**, 8770 (2018).
29. **R.C. Miller, D.A. Kleinman, and A.C. Gossard**: Observation of doubly resonant LO-phonon Raman scattering with GaAs-Al_xGa_{1-x} As quantum wells. *Solid State Commun.* **60**, 213 (1986).
30. **F. Cerdeira, E. Anastassakis, W. Kauschke, and M. Cardona**: Stress-induced doubly resonant Raman scattering in GaAs. *Phys. Rev. Lett.* **57**, 3209 (1986).
31. **A. Alexandrou, M. Cardona, and K. Ploog**: Doubly and triply resonant raman scattering by LO phonons in GaAs/AlAs superlattices. *Phys. Rev. B* **38**, 2196 (1988).
32. **S.I. Gubarev, T. Ruf, and M. Cardona**: Doubly resonant Raman scattering in the semimagnetic semiconductor $Cd_{0.95}Mn_{0.05}Te$. *Phys. Rev. B* **43**, 1551 (1991).
33. **I. Kupčić**: Triple-resonant two-phonon Raman scattering in graphene. *J. Raman Spectrosc.* **43**, 1 (2012).
34. **D. Yoon, Y.W. Son, and H. Cheong**: Strain-dependent splitting of the double-resonance raman scattering band in graphene. *Phys. Rev. Lett.* **106**, 1 (2011).
35. **P. Venezuela, M. Lazzeri, and F. Mauri**: Theory of double-resonant Raman spectra in graphene: Intensity and line shape of defect–induced and two-phonon bands. *Phys. Rev. B* **84**, 1 (2011).
36. **C. Thomsen and S. Reich**: Double resonant raman scattering in graphite. *Phys. Rev. Lett.* **85**, 5214 (2000).
37. **A. Grüneis, R. Saito, T. Kimura, L.G. Cançado, M.A. Pimenta, A.G. Jorio, A.G. Souza Filho, G. Dresselhaus, and M.S. Dresselhaus**: Determination of two-dimensional phonon dispersion relation of graphite by Raman spectroscopy. *Phys. Rev. B* **65**, 1 (2002).
38. **S. Reich and C. Thomsen**: Raman spectroscopy of graphite. *Philos. Trans. R. Soc., A* **362**, 2271 (2004).
39. **J. Maultzsch, S. Reich, and C. Thomsen**: Double-resonant Raman scattering in graphite: Interference effects, selection rules, and phonon dispersion. *Phys. Rev. B* **70**, 155403 (2004).
40. **L.G. Cançado, M.A. Pimenta, B.R.A. Neves, M.S.S. Dantas, and A. Jorio**: Influence of the atomic structure on the Raman spectra of graphite edges. *Phys. Rev. Lett.* **93**, 5 (2004).
41. **A.C. Ferrari**: Raman spectroscopy of graphene and graphite: Disorder, electron–phonon coupling, doping and nonadiabatic effects. *Solid State Commun.* **143**, 47 (2007).
42. **D.L. Mafra, G. Samsonidze, L.M. Malard, D.C. Elias, J.C. Brant, F. Plentz, E.S. Alves, and M.A. Pimenta**: Determination of LA and TO phonon dispersion relations of graphene near the Dirac point by double resonance Raman scattering. *Phys. Rev. B* **76**, 233407 (2007).
43. **L.G. Cançado, A. Jorio, E.H.M. Ferreira, F. Stavale, C.A. Achete, R.B. Capaz, M.V.O. Moutinho, A. Lombardo, T.S. Kulmala, and A.C. Ferrari**: Quantifying defects in graphene via Raman spectroscopy at different excitation energies. *Nano Lett.* **11**, 3190 (2011).
44. **K. Gołasa, M. Grzeszczyk, K.P. Korona, R. Bożek, J. Binder, J. Szczytko, A. Wysmołek, and A. Babiński**: Optical properties of molybdenum disulfide (MoS_2). *Acta Phys. Pol., A* **124**, 849 (2013).
45. **A. Berkdemir, H.R. Gutiérrez, A.R. Botello-Méndez, N. Perea-López, A.L. Elías, C-I. Chia, B. Wang, V.H. Crespi, F. López-Urías, J-C. Charlier, H. Terrones, and M. Terrones**: Identification of individual and few layers of WS_2 using Raman spectroscopy. *Sci. Rep.* **3**, 1755 (2013).

https://doi.org/10.1557/jmr.2019.167 Published online by Cambridge University Press

© Materials Research Society 2019

46. **A.A. Mitioglu, P. Plochocka, G. Deligeorgis, S. Anghel, L. Kulyuk, and D.K. Maude**: Second order resonant Raman scattering in single layer tungsten disulfide (WS_2). *Phys. Rev. B* **89**, 245442 (2014).
47. **H-L. Liu, H. Guo, T. Yang, Z. Zhang, Y. Kumamoto, C-C. Shen, Y-T. Hsu, L-J. Li, R. Saito, and S. Kawata**: Anomalous lattice vibrations of monolayer MoS_2 probed by ultraviolet Raman scattering. *Phys. Chem. Chem. Phys.* **17**, 14561 (2015).
48. **H. Guo, T. Yang, M. Yamamoto, L. Zhou, R. Ishikawa, K. Ueno, K. Tsukagoshi, Z. Zhang, M.S. Dresselhaus, and R. Saito**: Double resonance Raman modes in monolayer and few-layer $MoTe_2$. *Phys. Rev. B* **91**, 205415 (2015).
49. **W. Shi, M-L. Lin, Q-H. Tan, X-F. Qiao, J. Zhang, and P-H. Tan**: Raman and photoluminescence spectra of two–dimensional nanocrystallites of monolayer WS_2 and WSe_2. *2D Mater.* **3**, 025016 (2016).
50. **B.R. Carvalho, Y. Wang, S. Mignuzzi, D. Roy, M. Terrones, C. Fantini, V.H. Crespi, L.M. Malard, and M.A. Pimenta**: Intervalley scattering by acoustic phonons in two-dimensional MoS_2 revealed by doubley-resonance Raman spectroscopy. *Nat. Commun.* **8**, 14670 (2017).
51. **Q. Qian, Z. Zhang, and K.J. Chen**: Layer-dependent second-order Raman intensity of MoS_2 and WS_2: Influence of intervalley scattering. *Phys. Rev. B* **97**, 165409 (2018).
52. **J. Kutrowska-Girzycka, J. Jadczak, and L. Bryja**: The study of dispersive 'b'-mode in monolayer MoS_2 in temperature dependent resonant Raman scattering experiments. *Solid State Commun.* **275**, 25 (2018).
53. **T. Sekine, K. Uchinokura, T. Nakashizu, E. Matsuura, and R. Yoshizaki**: Dispersive Raman mode of layered compound 2H-MoS_2 under the resonant condition. *J. Phys. Soc. Jpn.* **53**, 811 (1984).
54. **A.M.M. Stacy and D.T.T. Hodul**: Raman spectra of IVB and VIB transition metal disulfides using laser energies near the absorption edges. *J. Phys. Chem. Solids* **46**, 405 (1985).
55. **C. Sourisseau, F. Cruege, M. Fouassier, and M. Alba**: Second-order Raman effects, inelastic neutron scattering and lattice dynamics in 2H-WS_2. *Chem. Phys.* **150**, 281 (1991).
56. **N.T. McDevitt, J.S. Zabinski, M.S. Donley, and J.E. Bultman**: Disorder-induced low-frequency Raman band observed in deposited MoS2 films. *Appl. Spectrosc.* **48**, 733 (1994).
57. **G.L. Frey, R. Tenne, M.J. Matthews, M.S. Dresselhaus, and G. Dresselhaus**: Raman and resonance Raman investigation of MoS_2 nanoparticles. *Phys. Rev. B* **60**, 2883 (1999).
58. **T. Livneh and E. Sterer**: Resonant Raman scattering at exciton states tuned by pressure and temperature in 2H-MoS_2. *Phys. Rev. B* **81**, 195209 (2010).
59. **Z. Lin, B.R. Carvalho, E. Kahn, R. Lv, R. Rao, H. Terrones, M.A. Pimenta, and M. Terrones**: Defect engineering of two-dimensional transition metal dichalcogenides. *2D Mater.* **3**, 022002 (2016).
60. **Z. Hu, Z. Wu, C. Han, J. He, Z. Ni, and W. Chen**: Two-dimensional transition metal dichalcogenides: Interface and defect engineering. *Chem. Soc. Rev.* **47**, 3100 (2018).
61. **M. Cardona and R. Merlin**: *Light Scattering in Solids I*., Vol. 8 (Springer, Berlin, Heidelberg, 1983).
62. **S. Mignuzzi, A.J. Pollard, N. Bonini, B. Brennan, I.S. Gilmore, M.A. Pimenta, D. Richards, and D. Roy**: Effect of disorder on Raman scattering of single-layer MoS_2. *Phys. Rev. B* **91**, 195411 (2015).
63. **H.L. Liu, S. Siregar, E.H. Hasdeo, Y. Kumamoto, C.C. Shen, C.C. Cheng, L.J. Li, R. Saito, and S. Kawata**: Deep-ultraviolet Raman scattering studies of monolayer graphene thin films. *Carbon* **81**, 807 (2015).
64. **L.M. Malard, D.L. Mafra, M.H.D. Guimarães, M.S.C. Mazzoni, and A. Jorio**: Group theory analysis of electrons and phonons in N-layer graphene systems. *Phys. Rev. B* **79**, 125426 (2008).
65. **C. Lee, X. Wei, J.W. Kysar, and J. Hone**: Measurement of the elastic properties and intrinsic strength of monolayer graphene. *Science* **321**, 385 (2008).
66. **S. Reich, J. Maultzsch, C. Thomsen, and P. Ordejón**: Tight-binding description of graphene. *Phys. Rev. B* **66**, 1 (2002).
67. **T.O. Wehling, A.M. Black-Schaffer, and A.V. Balatsky**: Dirac materials. *Adv. Phys.* **63**, 1 (2014).
68. **A.H. Castro Neto, F. Guinea, N.M.R. Peres, K.S. Novoselov, and A.K. Geim**: The electronic properties of graphene. *Rev. Mod. Phys.* **81**, 109 (2009).
69. **K.F. Mak, L. Ju, F. Wang, and T.F. Heinz**: Optical spectroscopy of graphene: From the far infrared to the ultraviolet. *Solid State Commun.* **152**, 1341 (2012).
70. **M.M. Lucchese, F. Stavale, E.H.M. Ferreira, C. Vilani, M.V.O. Moutinho, R.B. Capaz, C.A. Achete, and A. Jorio**: Quantifying ion-induced defects and Raman relaxation length in graphene. *Carbon* **48**, 1592 (2010).
71. **E.H. Martins Ferreira, M.V.O. Moutinho, F. Stavale, M.M. Lucchese, R.B. Capaz, C.A. Achete, and A. Jorio**: Evolution of the Raman spectra from single-, few-, and many-layer graphene with increasing disorder. *Phys. Rev. B* **82**, 125429 (2010).
72. **A. Eckmann, A. Felten, A. Mishchenko, L. Britnell, R. Krupke, K.S. Novoselov, and C. Casiraghi**: Probing the nature of defects in graphene by Raman spectroscopy. *Nano Lett.* **12**, 3925 (2012).
73. **S. Piscanec, M. Lazzeri, F. Mauri, A.C. Ferrari, and J. Robertson**: Kohn anomalies and electron–phonon interactions in graphite. *Phys. Rev. Lett.* **93**, 1 (2004).
74. **P. May, M. Lazzeri, P. Venezuela, F. Herziger, G. Callsen, J.S. Reparaz, A. Hoffmann, F. Mauri, and J. Maultzsch**: Signature of the two-dimensional phonon dispersion in graphene probed by double-resonant Raman scattering. *Phys. Rev. B* **87**, 075402 (2013).
75. **D.M. Basko, S. Piscanec, and A.C. Ferrari**: Electron–electron interactions and doping dependence of the two-phonon Raman intensity in graphene. *Phys. Rev. B* **80**, 165413 (2009).

https://doi.org/10.1557/jmr.2019.167 Published online by Cambridge University Press

© Materials Research Society 2019

76. **S. Bernard, E. Whiteway, V. Yu, D.G. Austing, and M. Hilke**: Experimental phonon band structure of graphene using C12 and C13 isotopes. *Phys. Rev. B* **86**, 085409 (2011).
77. **K.S. Novoselov, D. Jiang, F. Schedin, T.J. Booth, V.V. Khotkevich, S.V. Morozov, and A.K. Geim**: Two-dimensional atomic crystals. *Proc. Natl. Acad. Sci. U. S. A.* **102**, 10451 (2005).
78. **K.F. Mak, C. Lee, J. Hone, J. Shan, and T.F. Heinz**: Atomically thin MoS_2: A new direct-gap semiconductor. *Phys. Rev. Lett.* **105**, 136805 (2010).
79. **A. Splendiani, L. Sun, Y. Zhang, T. Li, J. Kim, C-Y. Chim, G. Galli, and F. Wang**: Emerging photoluminescence in monolayer MoS_2. *Nano Lett.* **10**, 1271 (2010).
80. **H.R. Gutiérrez, N. Perea-López, A.L. Elías, A. Berkdemir, B. Wang, R. Lv, F. López-Urías, V.H. Crespi, H. Terrones, and M. Terrones**: Extraordinary room-temperature photoluminescence in triangular WS_2 monolayers. *Nano Lett.* **13**, 3447 (2013).
81. **W. Zhao, Z. Ghorannevis, L. Chu, M. Toh, C. Kloc, P-H. Tan, and G. Eda**: Evolution of electronic structure in atomically thin sheets of WS_2 and WSe_2. *ACS Nano* **7**, 791 (2013).
82. **H.M. Hill, A.F. Rigosi, C. Roquelet, A. Chernikov, T.C. Berkelbach, D.R. Reichman, M.S. Hybertsen, L.E. Brus, and T.F. Heinz**: Observation of excitonic Rydberg states in monolayer MoS_2 and WS_2 by photoluminescence excitation spectroscopy. *Nano Lett.* **15**, 2992 (2015).
83. **R. Frisenda, Y. Niu, P. Gant, A.J. Molina-Mendoza, R. Schmidt, R. Bratschitsch, J. Liu, L. Fu, D. Dumcenco, A. Kis, D.P. De Lara, and A. Castellanos-Gomez**: Micro-reflectance and transmittance spectroscopy: A versatile and powerful tool to characterize 2D materials. *J. Phys. D: Appl. Phys.* **50**, 074002 (2017).
84. **K.F. Mak and J. Shan**: Photonics and optoelectronics of 2D semiconductor transition metal dichalcogenides. *Nat. Photonics* **10**, 216 (2016).
85. **K.F. Mak, K.L. McGill, J. Park, and P.L. McEuen**: Valleytronics. The Valley Hall effect in MoS_2 transistors. *Science* **344**, 1489 (2014).
86. **C. Mai, A. Barrette, Y. Yu, Y.G. Semenov, K.W. Kim, L. Cao, and K. Gundogdu**: Many-body effects in valleytronics: direct measurement of valley lifetimes in single-layer MoS_2. *Nano Lett.* **14**, 202 (2014).
87. **B.W.H. Baugher, H.O.H. Churchill, Y. Yang, and P. Jarillo-Herrero**: Optoelectronic devices based on electrically tunable p–n diodes in a monolayer dichalcogenide. *Nat. Nanotechnol.* **9**, 262 (2014).
88. **K.S. Novoselov, A. Mishchenko, A. Carvalho, and A.H. Castro Neto**: 2D materials and van der Waals heterostructures. *Science* **353**, aac9439 (2016).
89. **A.K. Geim and I.V. Grigorieva**: Van der Waals heterostructures. *Nature* **499**, 419 (2013).
90. **N. Mounet, M. Gibertini, P. Schwaller, D. Campi, A. Merkys, A. Marrazzo, T. Sohier, I.E. Castelli, A. Cepellotti, G. Pizzi, and N. Marzari**: Two-dimensional materials from high-throughput computational exfoliation of experimentally known compounds. *Nat. Nanotechnol.* **13**, 246 (2018).
91. **J. Gusakova, X. Wang, L.L. Shiau, A. Krivosheeva, V. Shaposhnikov, V. Borisenko, V. Gusakov, and B.K. Tay**: Electronic properties of bulk and monolayer TMDs: Theoretical study within DFT framework (GVJ–2e method). *Phys. Status Solidi* **214**, 1700218 (2017).
92. **J.A.A. Wilson and A.D.D. Yoffe**: The transition metal dichalcogenides discussion and interpretation of the observed optical, electrical and structural properties. *Adv. Phys.* **18**, 193 (1969).
93. **D.Y. Qiu, F.H. da Jornada, and S.G. Louie**: Optical spectrum of MoS_2: Many-body effects and diversity of exciton states. *Phys. Rev. Lett.* **111**, 216805 (2013).
94. **N. Zibouche, A. Kuc, J. Musfeldt, and T. Heine**: Transition-metal dichalcogenides for spintronic applications. *Ann. Phys.* **526**, 395 (2014).
95. **A.P.S. Gaur, S. Sahoo, J.F. Scott, and R.S. Katiyar**: Electron–phonon interaction and double–resonance Raman studies in monolayer WS_2. *J. Phys. Chem. C* **119**, 5146 (2015).
96. **J.M. Chen and C.S. Wang**: Second order Raman spectrum of MoS_2. *Solid State Commun.* **14**, 857 (1974).
97. **T. Livneh and J.E. Spanier**: A comprehensive multiphonon spectral analysis in MoS_2. *2D Mater.* **2**, 035003 (2015).
98. **Y. Gillet, S. Kontur, M. Giantomassi, C. Draxl, and X. Gonze**: Ab initio approach to second-order resonant Raman scattering including exciton–phonon interaction. *Sci. Rep.* **7**, 7344 (2017).
99. **G. Wang, M. Glazov, C. Robert, T. Amand, X. Marie, and B. Urbaszek**: Double resonant Raman scattering and valley coherence generation in monolayer WSe_2. *Phys. Rev. Lett.* **115**, 1 (2015).
100. **H-L. Liu, T. Yang, Y. Tatsumi, Y. Zhang, B. Dong, H. Guo, Z. Zhang, Y. Kumamoto, M-Y. Li, L-J. Li, R. Saito, and S. Kawata**: Deep-ultraviolet Raman scattering spectroscopy of monolayer WS_2. *Sci. Rep.* **8**, 11398 (2018).
101. **K. Gołasa, M. Grzeszczyk, P. Leszczyński, C. Faugeras, A.A.L. Nicolet, A. Wysmołek, M. Potemski, and A. Babiński**: Multiphonon resonant Raman scattering in MoS_2. *Appl. Phys. Lett.* **104**, 092106 (2014).
102. **H. Zeng, J. Dai, W. Yao, D. Xiao, and X. Cui**: Valley polarization in MoS_2 monolayers by optical pumping. *Nat. Nanotechnol.* **7**, 490 (2012).
103. **K.F. Mak, K. He, J. Shan, and T.F. Heinz**: Control of valley polarization in monolayer MoS_2 by optical helicity. *Nat. Nanotechnol.* **7**, 494 (2012).

https://doi.org/10.1557/jmr.2019.167 Published online by Cambridge University Press

© Materials Research Society 2019

104. **G. Kioseoglou, A.T. Hanbicki, M. Currie, A.L. Friedman, and B.T. Jonker**: Optical polarization and intervalley scattering in single layers of MoS_2 and $MoSe_2$. *Sci. Rep.* **6**, 25041 (2016).
105. **P. Dey, J. Paul, Z. Wang, C.E. Stevens, C. Liu, A.H. Romero, J. Shan, D.J. Hilton, and D. Karaiskaj**: Optical coherence in atomic-monolayer transition-metal dichalcogenides limited by electron–phonon interactions. *Phys. Rev. Lett.* **116**, 127402 (2016).
106. **W. Zhou, X. Zou, S. Najmaei, Z. Liu, Y. Shi, J. Kong, J. Lou, P.M. Ajayan, B.I. Yakobson, and J.C. Idrobo**: Intrinsic structural defects in monolayer molybdenum disulfide. *Nano Lett.* **13**, 2615 (2013).
107. **Z. Wu, Z. Luo, Y. Shen, W. Zhao, W. Wang, H. Nan, X. Guo, L. Sun, X. Wang, Y. You, and Z. Ni**: Defects as a factor limiting carrier mobility in WSe_2: A spectroscopic investigation. *Nano Res.* **9**, 3622 (2016).
108. **W.M. Parkin, A. Balan, L. Liang, P.M. Das, M. Lamparski, C.H. Naylor, J.A. Rodríguez-Manzo, A.T.C. Johnson, V. Meunier, and M. Drndić**: Raman shifts in electron-irradiated monolayer MoS_2. *ACS Nano* **10**, 4134 (2016).
109. **Z. Wu, W. Zhao, J. Jiang, T. Zheng, Y. You, J. Lu, and Z. Ni**: Defect activated photoluminescence in WSe_2 monolayer. *J. Phys. Chem. C* **121**, 12294 (2017).
110. **W. Shi, X. Zhang, X-L. Li, X-F. Qiao, J-B. Wu, J. Zhang, and P-H. Tan**: Phonon confinement effect in two-dimensional nanocrystallites of monolayer MoS_2 to probe phonon dispersion trends away from brillouin-zone center. *Chin. Phys. Lett.* **33**, 057801 (2016).
111. **H-P. Komsa, J. Kotakoski, S. Kurasch, O. Lehtinen, U. Kaiser, and A.V. Krasheninnikov**: Two-dimensional transition metal dichalcogenides under electron irradiation: Defect production and doping. *Phys. Rev. Lett.* **109**, 035503 (2012).
112. **J. Lu, A. Carvalho, X.K. Chan, H. Liu, B. Liu, E.S. Tok, K.P. Loh, A.H. Castro Neto, and C.H. Sow**: Atomic healing of defects in transition metal dichalcogenides. *Nano Lett.* **15**, 3524 (2015).
113. **H. Fang, M. Tosun, G. Seol, T.C. Chang, K. Takei, J. Guo, and A. Javey**: Degenerate n-doping of few–layer transition metal dichalcogenides by potassium. *Nano Lett.* **13**, 1991 (2013).
114. **K. Dolui, I. Rungger, C. Das Pemmaraju, and S. Sanvito**: Possible doping strategies for MoS_2 monolayers: An ab initio study. *Phys. Rev. B* **88**, 1 (2013).
115. **N. Saigal, I. Wielert, D. Čapeta, N. Vujičić, B. V Senkovskiy, M. Hell, M. Kralj, and A. Grüneis**: Effect of lithium doping on the optical properties of monolayer MoS_2. *Appl. Phys. Lett.* **112**, 121902 (2018).
116. **E. Asari, I. Kamioka, K.G. Nakamura, T. Kawabe, W.A. Lewis, and M. Kitajima**: Lattice disordering in graphite under rare-gas ion irradiation studied by Raman spectroscopy. *Phys. Rev. B* **49**, 1011 (1994).
117. **H. Richter, Z.P. Wang, and L. Ley**: The one phonon Raman spectrum in microcrystalline silicon. *Solid State Commun.* **39**, 625 (1981).
118. **I.H. Campbell and P.M. Fauchet**: The effects of microcrystal size and shape on the one phonon Raman spectra of crystalline semiconductors. *Solid State Commun.* **58**, 739 (1986).
119. **K. Ishioka, K.G. Nakamura, and M. Kitajima**: Phonon confinement in GaAs by defect formation studied by real-time Raman measurements. *Phys. Rev. B* **52**, 2539 (1995).
120. **C. Lee, B.G. Jeong, S.J. Yun, Y.H. Lee, S.M. Lee, and M.S. Jeong**: Unveiling defect-related Raman mode of monolayer WS_2 via tip-enhanced resonance Raman scattering. *ACS Nano* **12**, 9982 (2018).
121. **A. McCreary, J.R. Simpson, Y. Wang, D. Rhodes, K. Fujisawa, L. Balicas, M. Dubey, V.H. Crespi, M. Terrones, and A.R. Hight Walker**: Intricate resonant Raman response in anisotropic ReS_2. *Nano Lett.* **17**, 5897 (2017).
122. **D. Wolverson, S. Crampin, A.S. Kazemi, A. Ilie, and S.J. Bending**: Raman spectra of monolayer, few-layer, and bulk $ReSe_2$: An anisotropic layered semiconductor. *ACS Nano* **8**, 11154 (2014).
123. **X. Wang, N. Mao, W. Luo, H. Kitadai, and X. Ling**: Anomalous phonon modes in black phosphorus revealed by resonant Raman scattering. *J. Phys. Chem. Lett.* **9**, 2830 (2018).
124. **A. Favron, F.A. Goudreault, V. Gosselin, J. Groulx, M. Côté, R. Leonelli, J.F. Germain, A.L. Phaneuf-L'Heureux, S. Francoeur, and R. Martel**: Second-order Raman scattering in exfoliated black phosphorus. *Nano Lett.* **18**, 1018 (2018).

https://doi.org/10.1557/jmr.2019.167 Published online by Cambridge University Press

© Materials Research Society 2019